HHS Public Access

Author manuscript

*Sci Transl Med*. Author manuscript; available in PMC 2020 June 01.

Published in final edited form as:

*Sci Transl Med*. 2020 January 01; 12(524): . doi:10.1126/scitranslmed.aau5732.

# Prospective longitudinal atrophy in Alzheimer's disease correlates with the intensity and topography of baseline tau-PET

**Renaud La Joie**[1,*], **Adrienne V. Visani**[1], **Suzanne L. Baker**[2], **Jesse A. Brown**[1], **Viktoriya Bourakova**[1], **Jungho Cha**[1], **Kiran Chaudhary**[1], **Lauren Edwards**[1], **Leonardo Iaccarino**[1], **Mustafa Janabi**[2], **Orit Lesman-Segev**[1], **Zachary Miller**[1], **David C. Perry**[1], **James P. O'Neil**[2], **Julie Pham**[1], **Julio C. Rojas**[1], **Howard J. Rosen**[1], **William W. Seeley**[1], **Richard M. Tsai**[1], **Bruce L. Miller**[1], **William J. Jagust**[2,3], **Gil D. Rabinovici**[1,2,3,4]

[1]Memory and Aging Center, Department of Neurology, Weill Institute for Neurosciences, University of California, San Francisco, San Francisco, CA

[2]Molecular Biophysics and Integrated Bioimaging Division, Lawrence Berkeley National Laboratory, Berkeley, CA

[3]Helen Wills Neuroscience Institute, University of California Berkeley, Berkeley, CA

[4]Department of Radiology and Biomedical Imaging; University of California, San Francisco, San Francisco, CA

## Abstract

β-amyloid plaques and tau-containing neurofibrillary tangles are the two neuropathological hallmarks of Alzheimer's disease (AD) and are thought to play crucial roles in a neurodegenerative cascade leading to dementia. Both lesions can now be visualized *in vivo* using positron emission tomography (PET) radiotracers, opening new opportunities to study disease mechanisms and improve patients' diagnostic and prognostic evaluation. In a group of 32 patients at early symptomatic AD stages, we tested whether β-amyloid and tau-PET could predict subsequent brain atrophy measured using longitudinal magnetic resonance imaging acquired at the time of PET and 15 months later. Quantitative analyses showed that the global intensity of tau-, but not β-amyloid-PET signal predicted the rate of subsequent atrophy, independent of baseline cortical thickness. Additional investigations demonstrated that the specific distribution of tau-PET signal was a strong indicator of the topography of future atrophy at the single patient level and that the relationship between baseline tau-PET and subsequent atrophy was particularly strong in younger patients. These data support disease models in which tau pathology is a major driver of

[*]To whom correspondence should be addressed: Renaud.lajoie@ucsf.edu.

Author contribution

Study conceptualization: RLJ, GDR. Data acquisition and quality control: RLJ, AVV, SLB, VB, KC, LE, MJ, OLS, ZM, DCP, JPO, JP, JCR, HJR, RMT, BLM, WJJ, GDR. Data processing and methodology: RLJ, AVV, SLB, JAB, VB, JC, LE, LI, OLS, WWS. Data analysis: RLJ. Writing the original draft: RLJ. Reviewing and editing manuscript: all authors. Supervision: GDR. Project administration and resources: KC. Funding acquisition: RLJ, BLM, WJJ, GDR.

Competing interests

Renaud La Joie, Adrienne A. Visani, Jesse A. Brown, Viktoriya Bourakova, Jungho Cha, Kiran Chaudhary, Lauren Edwards, Leonardo Iaccarino, Mustafa Janabi, Orit Lesman-Segev, Zachary Miller, James P O'Neil and Julie Pham report no disclosure.

**Data and materials availability.** Most data associated with this study are available in the main text, supplementary datafile, or on neurovault for group-level voxelwise images (https://neurovault.org/collections/WLDODMCY/). Individual imaging data are not made freely available to protect patient privacy, but can be shared with investigators upon reasonable request.

local neurodegeneration and highlight the relevance of tau-PET as a precision medicine tool to help predict individual patient's progression and design future clinical trials.

## One Sentence Summary:

Tau imaging with [18F]Flortaucipir predicts the severity and topography of subsequent MRI cortical atrophy in patients with Alzheimer's disease.

## Introduction

Alzheimer's disease (AD) is characterized by the co-occurrence of β-amyloid (Aβ) deposition into extracellular plaques and neurofibrillary tangles composed of aggregated hyper-phosphorylated tau (1). The aggregation of Aβ and tau is thought to play a crucial role in a neurodegenerative cascade that results in the loss of neurons and synapses (2). The development of radiotracers binding to Aβ plaques (3) and paired helical filaments (PHF) of tau that comprise neurofibrillary tangles (4) allows the visualization and quantification of AD pathology in living patients using positron emission tomography (PET). Those imaging biomarkers offer an opportunity to improve patient diagnosis and to study the development of AD pathophysiology by describing the relationships between protein aggregation, neurodegeneration, and cognitive impairment.

Cross-sectional neuroimaging studies have demonstrated that lower brain volumes are more strongly associated with tau- than with Aβ-PET burden in patients with mild cognitive impairment and dementia (5). Moreover, studies examining the topography of neuroimaging biomarkers have indicated that the pattern of neurodegeneration (i.e. regions with low cortical volume/thickness (6, 7) or glucose hypometabolism (8, 9)) greatly resembles the pattern of elevated tau-PET, but not Aβ-PET signal. However, the spatial extent of tau-PET signal appears to exceed the extent of neurodegeneration (6, 8), suggesting that tau-PET elevation might precede, and potentially predict neurodegeneration. Converging evidence also suggests that the intensity and topography of tau-PET, but not Aβ-PET, are strongly associated with the severity of each patient's specific clinical deficits (10). In addition, earlier age of onset seems to be associated with higher tau-PET signal (8, 11), potentially accounting for the higher rates of brain atrophy observed in patients with early-onset AD compared to their older counterparts (12–14).

Since tau-PET imaging is a relatively novel technique, most previous studies have been based on cross-sectional data, which leads to technical and conceptual limitations. First, cross-sectional studies define neurodegeneration as low volume/metabolism, as they cannot directly measure decline in volume/metabolism over time. Resulting metrics are then biased by pre-existing inter-individual variability in cerebral anatomy and function (15). Second, cross-sectional designs do not allow direct observation of a chronological sequence of biomarker abnormalities. More recently, retrospective longitudinal studies (in which longitudinal MRI data were acquired before tau-PET acquisition) have also highlighted a close association between tau-PET and neurodegeneration (16, 17), but might be biased by the non-linear nature of atrophy over the disease course (18, 19).

In the present observational study, we prospectively assessed and compared the associations between baseline Aβ and tau-PET burden (using [11C]Pittsburgh Compound B (PIB) and [18F]Flortaucipir (FTP), respectively), and subsequent longitudinal atrophy in a group of patients at the early clinical stages of AD. Our primary hypothesis was that the tau deposition detected with FTP-PET drives, and therefore precedes regional neurodegeneration in early symptomatic AD. From a precision medicine perspective, we were interested in testing PET imaging's ability to predict neuroimaging changes at the individual patient level. Based on the cross-sectional evidence described above, we hypothesized that higher baseline FTP-, but not PIB-PET would be associated with higher atrophy rates, and that the topography of FTP-PET binding would predict the pattern of subsequent atrophy at the individual patient level. We had two secondary aims. First, we tested whether baseline PIB and FTP-PET data could help predict patients' clinical deterioration, measured with the clinical dementia rating scale sum of boxes (CDR-SB), a measure of disease severity based on functional decline (20). Lastly, we investigated whether the previously highlighted association between earlier age of onset and greater atrophy rates could be explained by baseline differences in tau burden.

## Results

The current study included 32 patients in early clinical stages of AD (Mild Cognitive Impairment or mild dementia, and a positive PIB-PET scan). All patients underwent structural MRI and PET with both PIB and FTP at the baseline visit, and a second structural MRI at a follow up visit (median time interval: 15 months). Two Siemens 3T-MRI scanners were used in this study (see Method and Discussion sections). Demographics are presented in Table 1. The sample was heterogeneous and included 6 patients fulfilling criteria for logopenic variant Primary Progressive Aphasia, lvPPA (21), and 3 patients meeting criteria for Posterior Cortical Atrophy, PCA (22)). Patients were between 49 and 83 years old at the time of PET scan (20 patients (63%) being under 65yo).

### At the group level, longitudinal atrophy is greater in regions with high baseline FTP binding

For each patient, baseline PET scans were processed to calculate Standardize Uptake Value Ratio (SUVR) maps (see (23) and the Methods section for more details). The two MRI scans were processed using a specific longitudinal pipeline (24) to derive a 3D map of jacobians representing annualized atrophy (jacobians were reversed so that positive values indicate tissue shrinkage over time). All maps were masked to restrict the investigations to the cortical gray matter (Figure S1), and analyzed in native or template space, depending on the analysis. We first created group-average images of PIB, FTP, and longitudinal atrophy using images warped to template space (Figure 1).

PIB binding predominated in medial areas (prefrontal and posterior cingulate/precuneus regions);signal was also elevated in lateral frontal and temporo-parietal cortices (Figure 1A). FTP binding was maximal at the temporo-parietal junction and the posterior cingulate / precuneus, and moderate in dorsal frontal, occipital and infero-medial temporal cortices (Figure 1A).

The pattern of longitudinal atrophy is shown in Figure 1B, as the group-average reversed jacobian map (higher values indicating higher atrophy rates) and as a statistical map based on a one-sample t-test performed on the 32 jacobian maps. Atrophy was maximal in temporo-parietal areas, posterior cingulate / precuneus and dorsal frontal areas, surviving stringent familywise error (FWE) correction ($p_{FWE}<0.001$) in those regions where baseline FTP-PET signal was particularly elevated.

## Patients with high baseline FTP-PET binding develop more severe cortical atrophy

We investigated the relationships between baseline cortical alterations (PIB SUVR, FTP SUVR, and cortical thickness) and the severity of subsequent atrophy across patients.

Figure 2 shows the associations between baseline global (mean of entire cortex) measures of PIB-SUVR, FTP-SUVR, and cortical thickness (values were derived from Freesurfer 5.3, Z-scored based on normative dataset (25), and reversed to higher values indicate lower baseline thickness), and overall cortical atrophy (average reversed cortical jacobian values). Longitudinal cortical atrophy was strongly associated with baseline FTP ($r_{FTP\text{-}atrophy}=0.670$, 95%CI [0.388, 0.841], $p<0.001$), in contrast with weaker correlations with baseline cortical PIB ($r_{PIB\text{-}atrophy}=0.291$, 95%CI [−0.029, 0.546], $p=0.07$), and baseline global cortical thickness ($r_{thickness\text{-}atrophy}=0.281$, 95%CI [−0.067, 0.586], $p=0.12$). Pairwise comparisons of correlations (based on bootstrapping of correlation coefficient pairs with 5,000 permutations) showed that longitudinal atrophy was more strongly correlated with FTP than PIB ($\Delta r=0.379$, 95%CI [0.121, 0.594], $p=0.004$), but the difference between $r_{FTP\text{-}atrophy}$ and $r_{thickness\text{-}atrophy}$ was not significant at $\alpha=0.05$ ($\Delta r=0.390$, 95%CI [−0.119, 0.821], $p=0.11$).

When including all three baseline predictors in a single multiple regression model to predict subsequent longitudinal atrophy, FTP remained significant (standardized $\beta=0.696$, $t=4.2$, $p<0.001$; versus $\beta=-0.083$, $t=-0.5$, $p=0.58$ for PIB and $\beta=0.173$, $t=1.3$, $p=0.22$ for thickness; see Table S1), and this full model did not perform better than a model including FTP only to predict longitudinal atrophy (Table S1).

## Voxelwise FTP-PET patterns predict maps of subsequent atrophy at the individual patient level

We next assessed whether the topography of PIB and FTP binding could help predict the pattern of atrophy at the individual patient level, using a voxelwise approach.

For each patient, the topographical similarity between 3D maps of PET binding and atrophy were quantified using a voxelwise spatial correlation approach restricted to a cortical mask, as previously described (26) and illustrated in Figure 3A (see Figure S1 for details on the preprocessing). Resulting spatial correlation coefficients (baseline PIB to longitudinal atrophy and baseline FTP to longitudinal atrophy) were then z-transformed to allow analysis at the group level (see Figure 3B). Across the 32 patients, spatial correlation between baseline PIB and subsequent atrophy was minimal: mean $z(r)=0.183$, 95%CI [0.131, 0.226] (percentile bootstrap CI based on 5,000 permutations), indicating 3% [2%, 5%] shared variance on average. In contrast, the spatial correlation between baseline FTP and longitudinal atrophy was high: mean $z(r)=0.780$, 95%CI [0.682, 0.859], indicating 43% [35%, 48%] shared variance on average. Spatial correlation with longitudinal atrophy was

significantly higher for baseline FTP than PIB (paired t-test conducted on the z(r) values: $t(31)=14.9$, $p<0.001$). It should be noted that correlations were higher for FTP than for PIB in all 32 patients, as shown in Figure 3B).

## Baseline tau-PET predicts longitudinal atrophy independent of baseline thickness

Our finding that baseline FTP-SUVR correlates with subsequent atrophy could be confounded by the fact that these regions are usually already atrophic at baseline, and that atrophy tends to accelerate locally. In addition, low cortical thickness at baseline could reduce the PET signal due to partial volume effects, and introduce additional noise in the measurements. We therefore conducted additional analyses to assess the potential confounding effect of "baseline atrophy" on the association between FTP-PET and subsequent atrophy at a regional level. This set of analyses was conducted using regions of interests, enabling the use of partial volume corrected (PVC) PET data. Each patient's cortex was segmented into 68 regions of interest (ROI) using Freesurfer 5.3, and the average cortical thickness was extracted from the baseline MRI for each ROI. For each patient, cortical thickness values were converted to a Z-score (based on normative data, see methods) to be used as indicators of baseline neurodegeneration. Average baseline FTP-$SUVR_{PVC}$, and jacobian values were extracted from each ROI as well (see Figure S2 for details on the preprocessing and Figure 4A to visualize group averages).

The spaghetti plots in Figure 4B show that, for most patients, regions with higher baseline FTP-$SUVR_{PVC}$ and, to a smaller extent, lower baseline cortical thickness had higher atrophy rates. Linear mixed effect models (LMEMs) were used to test the respective contribution of each baseline measure to longitudinal atrophy. All ROIs from all patients were included in LMEMs (68 x 32 = 2,176 entries), with random slopes and intercepts for both ROI and patient factors (See Table S2 for further details on model specifications and results). Separate LMEMs were first conducted for each predictor, and both were significant ($p<0.001$, see Figure 4B, right bottom panel), although $FTP_{PVC}$ was a stronger predictor ($t=12.6$, marginal $R^2=0.444$, conditional $R^2=0.785$) than baseline thickness ($t=5.1$, marginal $R^2=0.057$, conditional $R^2=0.610$). However, when entering both predictors in the same model (Figure 4B, bottom line), only $FTP_{PVC}$ was significant ($t=11.9$, $p<0.001$, versus $t=-1.7$, $p=0.09$ for thickness). In addition, this full model roughly explained the same amount of variance (marginal $R^2=0.426$, conditional $R^2=0.800$) as the model including baseline $FTP_{PVC}$ only, and had a slightly decreased AIC value (−15,579 versus −15,498; see Table S2), indicating that adding baseline thickness only minimally improved the overall model fit.

The conclusions of the LMEMs were very similar when using non-PVC PET data, and when including baseline PIB-SUVR in the model (see Figure S3).

## Baseline tau-PET is more strongly associated with follow up than baseline cortical thickness

We hypothesized that baseline tau PET will correlate more strongly with cortical thickness measured at follow up than at baseline, consistent with a conceptual model in which tau deposition precedes neurodegeneration.

Figure 5A shows that, at the group level, baseline tau burden (global cortical FTP-$SUVR_{PVC}$) correlated more strongly with global cortical thinning (reversed Z-scored thickness) measured at follow up than baseline (r=0.431, 95%CI [0.166, 0.663] versus r=0.168, 95%CI [−0.150, 0.480], Δr=0.263, bootstrapped 95%CI [0.026, 0.517], p=0.026).

We also tested the spatial similarity between baseline tau-PET and cortical thinning measured at each timepoint (Figure 5B). The method was similar to that presented in Figure 3, except that the patient-level analysis was conducted using ROIs rather than voxelwise, enabling to calculate Z-score thickness values as mentioned above (see Figure S2). Across the 32 patients, baseline $FTP_{PVC}$ spatially correlated with concurrent cortical thickness: mean spatial correlation z(r) = 0.787, 95%CI [0.681, 0.876], indicating 43% [35%, 50%] shared variance on average. Yet, the spatial correlation was higher between baseline $FTP_{PVC}$ and follow-up thickness patterns: mean z(r) = 0.833, 95%CI [0.727, 0.921], indicating 47% [39%, 53%]; paired t-test on the z(r) values: t(31)=2.86, p=0.008.

## Longitudinal precuneus atrophy parallels clinical decline

The CDR-SB was used to measure clinical progression; to control for variations in clinical follow-up duration (mean = 15.0 months, min = 11.1, max = 23.7), changes in CDR-SB were annualized ((follow-up – baseline) / time interval). On average, CDR-SB increased by 1.6 ± 2.0 points per year (one-sample t-test: t(31)=4.52, p<0.001).

Annualized CDR-SB increase was poorly correlated with global cortical measures of baseline PIB SUVR (r=−0.125, p=0.51), FTP SUVR (r=−0.041, p=0.80), cortical thickness (r=0.006, p=0.95), or longitudinal atrophy (r=0.095, p=0.65; see Figure S4 for 95%CI and scatterplots). Voxelwise analyses showed that increase in CDR-SB over time was associated with longitudinal atrophy in the precuneus/posterior cingulate area (surviving FWE-correction at the voxel level; see Figure S4). In contrast, no regional association was found with any of the three baseline predictors (based on the $p_{uncorrected}$<0.001 threshold).

## Earlier disease onset is associated with higher tau burden and thus more rapid atrophy

Older age at baseline was associated with lower baseline abnormalities (Figure S5), although the correlation only reached statistical significance (at α=0.05) for baseline FTP-SUVR (r=−.572, p=0.002), but not baseline PIB-SUVR (r=−0.313, p=0.07) and baseline thickness (r=−0.224, p=0.12, see Figure 6A for 95%CI and scatterplots). In addition, older patients had lower rates of atrophy (correlation between age and reversed average cortical jacobian: r=−0.542, p=0.006 Figure 6A). When including both patient's age and baseline cortical FTP-SUVR in a multiple regression model, FTP remained highly predictive of longitudinal atrophy (standardized β=0.536, p=0.003), while the effect of age was reduced (standardized β=−0.235, p=0.16). Mediation analyses further showed that the relationship between patient's age and longitudinal rate of atrophy was at least partly mediated by baseline cortical FTP-SUVR (Figure 6A). No mediation effect was found using baseline PIB-SUVR or baseline cortical thickness (see Figure S6).

Voxelwise analyses showed that both FTP-SUVR and longitudinal atrophy decreased with greater patient age throughout the brain (Figure 6B), and most strongly in the fronto-parietal

areas where correlations reached statistical significance ($p_{unc}$<0.001 at the voxel level with $p_{FWE}$<0.05 at the cluster level, see Figure S7).

Finally, the spatial similarity between baseline FTP-SUVR maps and patterns of subsequent atrophy (quantified at the individual patient level using the voxelwise spatial correlation method described in Figure 3) decreased with age (r=−0.471, p=0.005), see Figure 6B. Spatial correlation values went from an estimated z(r)~0.9 at age 55 ($R^2$=52% shared variance) to z(r)~0.63 at age 75 ($R^2$=31% shared variance). The spatial correlation between baseline PIB and longitudinal atrophy was low regardless of patient's age (r=−0.253, p=0.13, see Figure S5 for 95%CI and scatterplots).

## Discussion

In this prospective longitudinal neuroimaging study conducted in patients at early clinical stages of AD, we investigated the associations between baseline PET measures of tau and Aβ burden and subsequent neurodegeneration measured as MRI atrophy over time. In line with our original hypotheses, we found that baseline tau PET, but not Aβ-PET, predicted the degree and spatial distribution of cortical atrophy over the subsequent year.

The association between baseline FTP-PET and subsequent atrophy, and notably the topographical similarity between the two patterns, was a strong and robust finding. Indeed, the association was found at both the group (Figure 1, Figure 2) and the individual patient levels (Figure 3, Figure 4), and using complementary voxelwise (Figure 3) and ROI-based (Figures 4 and 5, Figure S3) approaches. The predictive value of the baseline tau-PET pattern on future atrophy remained substantial even after adjusting for baseline cortical thickness, with tau-PET explaining ~40% of unique variance in longitudinal atrophy. Finally, although cross sectional relationships can be found between tau-PET and concurrent neurodegeneration, we showed that tau-PET more closely resembles neurodegeneration at a future time point (Figure 5). Taken together, these longitudinal results expand on previous findings from post-mortem and cross-sectional studies, by providing prospective evidence that the aggregation of tau predicts future neurodegeneration in patients with biomarker-confirmed AD. These results support a sequential relationship between tau fibrillar aggregates and downstream degeneration. This directionality is in line with a recent longitudinal tau-PET study from our group showing that, at the clinical stage of AD, tau pathology and brain atrophy progress in different regions, likely reflecting a phase shifting, with tau elevation locally preceding atrophy (27).

Multiple studies (28–31) previously reported that baseline CSF concentration of tau were associated with higher atrophy rates in heterogeneous groups of patients, though contradicting results exist (32, 33). Our finding of an association between global cortical FTP and global cortical atrophy (Figure 2A) confirms that this relationship is not driven by the inclusion of AD (high biomarker, high atrophy) and controls or non-AD (low biomarker, low atrophy) patients, but exists within a group of patients with biomarker-confirmed AD. The replicability of the tau biomarker/subsequent atrophy association across biomarker types (fluid versus imaging) is also consistent with the relationships found between PET and CSF measures of tau (23, 34, 35). The topographical information embedded in the PET data

constitutes a major advantage compared to CSF markers. Indeed, we demonstrated that tau-PET is not only predictive of *how much* but also of *where* atrophy will occur, which has major implications for patient prognosis and clinical trials.

Our findings suggest that tau-PET could be useful for the design of clinical trials, and notably could increase the ability to detect a treatment effect, even over a relatively short timeframe (36, 37). First, tau-PET could be used to enrich trials with patients with tau PET signal predictive of upcoming atrophy, or to stratify patients in trials based on the degree of expected atrophy in the upcoming year. Second, tau-PET could help determine how (i.e. where) atrophy should be measured to maximize study sensitivity. In fact, a major issue of using MRI to monitor disease progression is the inter-individual heterogeneity in atrophy patterns (38), even when selecting patients with a classic amnestic phenotype as in the Alzheimer's Disease Neuroimaging Initiative (12, 39). A given generic ROI (e.g. the hippocampus) would not optimally capture every patient's brain atrophy (e.g. patients with "hippocampal-sparing AD" (38, 40) ). Alternative options exist to maximize detection of AD atrophy using data-driven ROIs (41) or adapting the ROI to specific phenotypes (42), but our data suggest that PET could be used to create patient-tailored, FTP-informed ROIs for atrophy detection. This approach could capture tau-mediated neurodegeneration in every patient in a more optimal manner, agnostic of any *a priori* assumptions. Alternatively, the tight relationship between tau and atrophy might imply that, in regions with elevated tau-PET signal, the pathological cascade leading to neurodegeneration has already been triggered and that neurodegeneration processes are now uncoupled from tau pathology. In that case, anti-tau therapies could be more effective in preventing atrophy in regions with low-to-mild tau-PET signal, while atrophy in high tau-PET regions would be difficult to modify with anti-tau therapies.

Clinical decline measured with the CDR-SB was associated with atrophy in the precuneus, but was not correlated with baseline FTP-PET. This weak relationship might be related to methodological factors: the small sample size, the intrinsic noise of measuring clinical progression based on 2 timepoints, or the use of memory-centric CRD-SoB in a clinically diverse cohort like ours that includes language, and visuospatial-predominant AD phenotypes. Alternatively, the lack of correlation with FTP could also reflect the indirect relationship between tau pathology and clinical deficits that is thought to be at least partly mediated by brain degeneration (10).

In contrast to tau-PET, neither the burden nor topography of Aβ-PET were strong predictors of future atrophy. This is consistent with multiple reports that Aβ-PET has no or weak relationships with the patterns of neurodegeneration or clinical deficits at symptomatic stages (8, 43), although associations might be found at earlier (preclinical) stage (44). The quantitative and topographical dissociation between Aβ and neurodegeneration is also consistent with autopsy data (45, 46). To our knowledge, the relationships between baseline volume or thickness and future atrophy has not been thoroughly investigated, but studies have suggested that atrophy accelerates over time, before decelerating in later stages (18, 19). This non-linear relationship might explain why we could not identify consistent and robust relationships between baseline MRI findings and subsequent atrophy.

Baseline tau-PET accounted for ~40–50% of the severity and topography of subsequent atrophy in our cohort. Future investigations will be needed to study additional predictors of atrophy (e.g. inflammation (47), non-local effects of pathology (48, 49) or additional brain pathologies (50)) in order to further our understanding of the complex mechanisms underlying neurodegeneration in AD.

Our analyses identified patient's age as an important factor regarding not only the severity of tau burden and brain atrophy, but also the relationship between pathology and longitudinal atrophy. First, we replicated previous findings that later age of disease onset is associated with lower tau-PET burden (8, 11) and longitudinal atrophy rates (12–14). Moreover, we showed that the spatial association between FTP and longitudinal atrophy sharply decreased with patient's age (Figure 5), in line with a recent cross-sectional study (51). Altogether, these results are consistent with the idea that early-onset AD might constitute a more pure form of AD in which neurodegeneration is mainly driven by AD pathology, while later-onset clinical AD is multifactorial, associated with distinctive risk factors, and related to more frequent co-morbidities and co-pathologies (52, 53). Previous clinico-pathological studies showed that the relationship between AD neuropathology and dementia decreased in older patients (54). Altogether, growing evidence suggests that potential disease-modifying drugs that specifically target AD neuropathology may benefit patients with earlier-onset AD more than older patients.

A number of study features and limitations should be highlighted to appropriately interpret our results. First, it should be noted that PET signal is only a proxy for underlying pathology, and while post-mortem studies suggest FTP binds to paired helical filaments of tau (55, 56), "off target" signal unrelated to tau in basal ganglia (57, 58) and in some tau-negative conditions (59, 60) raise questions about specificity. Second, the sample size was modest, though similar to previous cross-sectional tau-PET/atrophy association studies. The use of complementary robust statistical approaches, and the inspection of all scatterplots and images clearly showed that results were not influenced by outliers. Third, the patients included in our study constitute an academic-based cohort of diverse and relatively young patients, which may limit generalizability. It should be noted that the results remained unchanged when excluding non-amnestic variants (language or visuo-spatial phenotypes of AD, see Figure S8). Fourth, our cohort encompassed early clinical stages of AD, and the results cannot be extrapolated to earlier (i.e. preclinical) or more severe stages of the disease, when neurodegeneration might be associated or driven by distinct mechanisms. Fifth, due to the recent development of FTP, patients only had one follow up MRI after the baseline visit, and additional time points would enable a more precise characterization of atrophy trajectories. Future studies will be needed to determine if the prognostic value of baseline tau-PET over longer follow-up. Similarly, clinical decline was evaluated based on two time points only, and more data would be needed to improve signal to noise; the limited available time points, together with the heterogeneity of the cohort, might account for the lack of associations between baseline tau-PET and clinical decline. Lastly, our patients underwent MRI scanning on 2 different Siemens 3T scanners, which might have added noise to the estimation of longitudinal atrophy. However, further analyses showed that the present results were found independently of MRI scanning protocol (Figure S9).

In summary, our study illustrates the potential of PET imaging to identify the pathological drivers of neurodegeneration in AD, and to help predict individual patients' future evolution. These results outline the robust local relationships between accumulation of tau-containing paired helical filament and neurodegeneration, emphasizing tau as a relevant target for disease-modifying drugs at this early clinical stage (61). Additional studies will be needed to extend our approach to larger cohorts, notably considering additional disease stages, older age-of-onset, and longer follow up duration.

## Materials & Methods

### Experimental design

The main objective of this study was to test whether amyloid and tau-PET could predict future brain atrophy in patients at symptomatic stages of AD. Data was derived from an ongoing longitudinal observational study including repeated MRI, PIB-PET and FTP-PET in patients with a clinical diagnosis of AD at the mild cognitive impairment or dementia stage. No power analysis was performed prior to the study but the sample size is within the range of previous papers assessing relationships between tau-PET and brain volume in symptomatic patients (6–7,17). Data preprocessing steps were performed using automated pipeline agnostic of the baseline tau- and amyloid-PET data. Quality control of the preprocessing steps was done blind to the baseline PET measures. No outlier was detected and all data was included in all analyses and plotted on each figure.

### Patients

All patients underwent a comprehensive clinical evaluation (10) at the UCSF Memory and Aging Center. We selected patients who i) had a clinical diagnosis of AD (at either the Mild Cognitive Impairment or dementia stage(62, 63)), ii) had undergone 3 Tesla structural MRI, FTP-PET and PIB-PET at their baseline visit, iii) had a positive PIB-PET (based on visual read (64)), and iv) had a follow up 3T MRI at least 9 months after the first visit. By 12/01/2018, 36 patients fulfilled these criteria, but 4 were excluded because of movement artifacts on an MRI and/or failure of the longitudinal MRI pipeline. The remaining 32 patients were included in the analyses.

Written informed consent was obtained from all patients or their surrogates. The study was approved by the University of California (San Francisco and Berkeley) and Lawrence Berkeley National Laboratory (LBNL) institutional review boards for human research.

### Image acquisition

T1-weighted magnetization prepared rapid gradient echo (MPRAGE) MRI sequences were acquired at UCSF, either on a 3T Siemens Tim Trio or a 3T Siemens Prisma Fit scanner. Both scanners had very similar acquisition parameters (sagittal slice orientation; slice thickness = 1.0 mm; slices per slab = 160; in-plane resolution = 1.0x1.0 mm; matrix = 240x256; repetition time = 2,300 ms; inversion time = 900 ms; flip angle = 9°), although echo time slightly differed (Trio: 2.98 ms; Prisma: 2.9 ms).

PET data were acquired on a Siemens Biograph PET/CT scanner at the Lawrence Berkeley National Laboratory (LBNL). Both radiotracers were synthesized and radiolabeled at LBNL's Biomedical Isotope Facility. In this paper, we analyzed PET data that was acquired from 50–70 min after the injection of ~15 mCi of PIB (four 5-min frames), and 80–100 min after the injection of ~10mCi of FTP (four 5-min frames). A low-dose CT scan was performed for attenuation correction prior to PET acquisition, and PET data were reconstructed using an ordered subset expectation maximization algorithm with weighted attenuation and smoothed with a 4 mm Gaussian kernel with scatter correction (calculated image resolution 6.5 x 6.5 x 7.25 mm based on Hoffman phantom).

### SUVR calculation

Each patient's baseline MRI was segmented using Freesurfer 5.3 (http://surfer.nmr.mgh.harvard) and Statistical Parametric Mapping 12 (SPM12, Wellcome Department of Imaging Neuroscience, Institute of Neurology, London, England) to create tracer-specific PET reference regions. PET frames were realigned, averaged and coregistered onto their corresponding MRI. SUVR images were created using Freesurfer-defined cerebellar gray matter for PIB-PET. For FTP, Freesurfer segmentaton was combined with the SUIT template (65) (which was reverse normalized to each patient individual space using SPM12) to only include inferior cerebellum voxels therefore avoiding contamination from off target binding in the dorsal cerebellum (58, 66).

### Longitudinal pipeline and voxelwise analyses

For each patient, the baseline and follow up MRIs were processed using SPM12 pairwise longitudinal registration (24), creating a within-patient mid-point average MRI and a 3D Jacobian rate map reflecting an annualized measure of volumetric change. In this original Jacobian map, negative values indicate contraction over time (e.g. classically in the brain), whereas positive values indicate expansion (e.g. in the ventricles). The Jacobian maps were reversed (i.e. multiplied by −1) so higher values in the cortex indicate greater atrophy. PIB and FTP-SUVR images were moved from baseline MRI space to the mid-point average MRI space using SPM12's deformation toolbox, to be aligned with the Jacobian rate map.

The mid-point average MRI was then segmented into gray matter, white matter and cerebrospinal fluid. The tissue segments were used to derive a binary gray matter mask, that was later masked to exclude basal ganglia (because of FTP off-target binding (57) and relative sparing in AD) and cerebellum (i.e. PET reference region) using the Hammers atlas (67), resulting in a binary cerebral cortical mask (see Figure S1 for illustration).

The reversed Jacobian rate map and the PET-SUVR images were finally smoothed within this mask using AFNI 3dBlurInMask command and applying differential kernels (4mm for PET, 8mm for Jacobians) so all three images had equivalent final smoothness (Figure S1). These images were used to calculate spatial correlations between patterns of atrophy (Jacobian values) and PET binding (Figure 3).

PIB, FTP and Jacobian maps from all patients were warped to MNI space using the deformation parameters estimated during the mid-point average MRI segmentation step and averaged to create across patient averages for PIB SUVR, FTP SUVR and jacobians (Figure

1). Template warped jacobian maps were entered in a voxelwise one-sample t-test to detect areas of significant atrophy (reversed jacobians > 0) over time (Figure 1).

All voxelwise results were presented using an uncorrected voxel threshold of $p<.001$ combined with a corrected cluster threshold of $p_{FWE}<0.05$; voxels that reached more conservative voxel-level thresholds ($p_{FWE}<0.05$ and $p_{FWE}<0.001$) were also highlighted.

### Freesurfer segmentation and ROI analyses

In order to quantify baseline cortical neurodegeneration (i.e. in a cross sectional design), we used the FreeSurfer segmentation outputs derived from the previous step (see "SUVR calculation" section above) and based on the first MRI. The average thickness measure of each of the 68 cortical ROIs was extracted from each patient's FreeSurfer directory and converted into a Z-score based on the code and the data provided by Potvin et al (25). Briefly, patients' thickness values were converted into Z-scores denoting the deviation from their expected values, as calculated based on the patient's characteristics (age, sex, estimated total intracranial volume, scanner manufacturer, and magnetic field strength) and a normative multicentric sample of 2,713 healthy controls aged 18 to 94 years. This approach was previously used to quantify cortical thickness in AD (68).

To assess the correlation between the patterns of baseline GM and subsequent atrophy (i.e. are regions that shrink over time already abnormally small at baseline?), we extracted the average SPM12-generated jacobian values from each of the 68 Freesurfer ROIs for each patient. Average FTP-PET SUVR values were extracted from all 68 ROIs using a partial volume correction (PVC) algorithm based on geometric transfer matrix technique (see (58, 66)). Linear mixed effect models were run including all ROIs from all patients (including random slopes and intercepts for both factors), with longitudinal atrophy (jacobian values) as the dependent variable, and baseline thickness Z-score and/or FTP-$SUVR_{PVC}$ as predictors.

### Statistical analyses

All statistical analyses were conducted using Matlab 2015a (The MathWorks, Inc., www.mathworks.com/) and the Robust correlation toolbox (69) to calculate Pearson correlation estimates and percentile bootstrap CI (from which p values were derived). Jamovi (www.jamovi.org) was used to conduct multiple regressions, ANOVAs, mediation analyses, and linear mixed effect models using dedicated modules. Details about each specific analysis are provided with the description of the analyses in the result section or supplementary materials.

Imaging results were displayed on 3-dimensional brain surfaces using BrainNetViewer(70) and ggseg (https://lcbc-uio.github.io/ggseg/).

Supplementary Datafile 1 contains most of the data used in the analyses presented in the article.

## Supplementary Material

Refer to Web version on PubMed Central for supplementary material.

## Acknowledgments

The authors are grateful to the patients and their caregivers for their participation in the study.

Avid Radiopharmaceuticals enabled use of the [18F]Flortaucipir tracer by providing precursor, but did not provide direct funding and was not involved in data analysis or interpretation

**Funding**. Alzheimer's Association (AARF-16-443577 to R.L.J), National Institute on Aging grants (R01-AG045611; to G.D.R.; P50-AG023501; to B.L.M. and G.D.R; P01-AG19724 to W.J.J., B.L.M and G.D.R.); Tau Consortium (to G.D.R. and W.J.J); State of California Department of Health Services Alzheimer's Disease Research Centre of California grant (04-33516; to B.L.M)

David Perry receives support from NIH (K23AG045289)

Julio C. Rojas receives support from NIH (R01 AG038791 PI, Adam Boxer) and travel funds from Eli Lilly.

Suzanne L. Baker consults for Genentech

William Seeley receives research support from NIH/NIA and has received consulting fees from Merck, Inc., Biogen Idec, and Bristol-Myers Squibb. Howard J Rosen receives research support from NIH/National Institute on Aging, RO1 AG032306 (PI), PO1 AG019724 (Core leader), AG045333 (PI), AG023501 (Core leader)

Richard Tsai receives research support from the University of California. He also consulted for ExpertConnect and Grifols.

Bruce L Miller receives research support from the NIH/NIA and the Centers for Medicare & Medicaid Services (CMS) as grants for the Memory and Aging Center. As an additional disclosure, Dr. Miller serves as Medical Director for the John Douglas French Foundation; Scientific Director for the Tau Consortium; Director/Medical Advisory Board of the Larry L. Hillblom Foundation; Scientific Advisory Board Member for the National Institute for Health Research Cambridge Biomedical Research Centre and its subunit, the Biomedical Research Unit in Dementia (UK); and Board Member for the American Brain Foundation (ABF).

William J Jagust has served as a consultant to BioClinica, Genentech, and Novartis Pharmaceuticals.

Gil D Rabinovici receives research support from Avid Radiopharmaceuticals, GE Healthcare, and Life Molecular Imaging, and has received consulting fees or speaking honoraria from Axon Neurosciences, Roche, Eisai, Genentech, Merck.

## References

1. Hyman BT, Phelps CH, Beach TG, Bigio EH, Cairns NJ, Carrillo MC, Dickson DW, Duyckaerts C, Frosch MP, Masliah E, Mirra SS, Nelson PT, Schneider JA, Thal DR, Thies B, Trojanowski JQ, Vinters HV, Montine TJ, National Institute on Aging–Alzheimer's Association guidelines for the neuropathologic assessment of Alzheimer's disease, Alzheimers Dement 8, 1–13 (2012). [PubMed: 22265587]
2. Duyckaerts C, Delatour B, Potier M-C, Classification and basic pathology of Alzheimer disease, Acta Neuropathol. (Berl.) 118, 5–36 (2009). [PubMed: 19381658]
3. Klunk WE, Engler H, Nordberg A, Wang Y, Blomqvist G, Holt DP, Bergström M, Savitcheva I, Huang G, Estrada S, Ausén B, Debnath ML, Barletta J, Price JC, Sandell J, Lopresti BJ, Wall A, Koivisto P, Antoni G, Mathis CA, Långström B, Imaging brain amyloid in Alzheimer's disease with Pittsburgh Compound-B, Ann. Neurol 55, 306–319 (2004). [PubMed: 14991808]
4. Chien DT, Bahri S, Szardenings AK, Walsh JC, Mu F, Su M-Y, Shankle WR, Elizarov A, Kolb HC, Early clinical PET imaging results with the novel PHF-tau radioligand [F-18]-T807, J. Alzheimers Dis. JAD 34, 457–468 (2013). [PubMed: 23234879]

5. Cho H, Choi JY, Hwang MS, Lee JH, Kim YJ, Lee HM, Lyoo CH, Ryu YH, Lee MS, Tau PET in Alzheimer disease and mild cognitive impairment, Neurology 87, 375–383 (2016). [PubMed: 27358341]

6. Iaccarino L, Tammewar G, Ayakta N, Baker SL, Bejanin A, Boxer AL, Gorno-Tempini ML, Janabi M, Kramer JH, Lazaris A, Lockhart SN, Miller BL, Miller ZA, O'Neil JP, Ossenkoppele R, Rosen HJ, Schonhaut DR, Jagust WJ, Rabinovici GD, Local and distant relationships between amyloid, tau and neurodegeneration in Alzheimer's Disease, NeuroImage Clin 17, 452–464 (2018). [PubMed: 29159058]

7. Nasrallah IM, Chen YJ, Hsieh M-K, Phillips JS, Ternes K, Stockbower GE, Sheline Y, McMillan CT, Grossman M, Wolk DA, 18F-Flortaucipir PET/MRI Correlations in Nonamnestic and Amnestic Variants of Alzheimer Disease, J. Nucl. Med. Off. Publ. Soc. Nucl. Med 59, 299–306 (2018).

8. Ossenkoppele R, Schonhaut DR, Schöll M, Lockhart SN, Ayakta N, Baker SL, O'Neil JP, Janabi M, Lazaris A, Cantwell A, Vogel J, Santos M, Miller ZA, Bettcher BM, Vossel KA, Kramer JH, Gorno-Tempini ML, Miller BL, Jagust WJ, Rabinovici GD, Tau PET patterns mirror clinical and neuroanatomical variability in Alzheimer's disease, Brain J. Neurol 139, 1551–1567 (2016).

9. Dronse J, Fliessbach K, Bischof GN, von Reutern B, Faber J, Hammes J, Kuhnert G, Neumaier B, Onur OA, Kukolja J, van Eimeren T, Jessen F, Fink GR, Klockgether T, Drzezga A, In vivo Patterns of Tau Pathology, Amyloid-β Burden, and Neuronal Dysfunction in Clinical Variants of Alzheimer's Disease, J. Alzheimers Dis. JAD 55, 465–471 (2017). [PubMed: 27802224]

10. Bejanin A, Schonhaut DR, La Joie R, Kramer JH, Baker SL, Sosa N, Ayakta N, Cantwell A, Janabi M, Lauriola M, O'Neil JP, Gorno-Tempini ML, Miller ZA, Rosen HJ, Miller BL, Jagust WJ, Rabinovici GD, Tau pathology and neurodegeneration contribute to cognitive impairment in Alzheimer's disease, Brain J. Neurol 140, 3286–3300 (2017).

11. Pontecorvo MJ, Devous MD, Navitsky M, Lu M, Salloway S, Schaerf FW, Jennings D, Arora AK, McGeehan A, Lim NC, Xiong H, Joshi AD, Siderowf A, Mintun MA, 18F-AV-1451-A05 investigators, Relationships between flortaucipir PET tau binding and amyloid burden, clinical diagnosis, age and cognition, Brain J. Neurol 140, 748–763 (2017).

12. Fiford CM, Ridgway GR, Cash DM, Modat M, Nicholas J, Manning EN, Malone IB, Biessels GJ, Ourselin S, Carmichael OT, Cardoso MJ, Barnes J, Alzheimer's Disease Neuroimaging Initiative, Patterns of progressive atrophy vary with age in Alzheimer's disease patients, Neurobiol. Aging 63, 22–32 (2018). [PubMed: 29220823]

13. Cho H, Jeon S, Kang SJ, Lee J-M, Lee J-H, Kim GH, Shin JS, Kim CH, Noh Y, Im K, Kim ST, Chin J, Seo SW, Na DL, Longitudinal changes of cortical thickness in early- versus late-onset Alzheimer's disease, Neurobiol. Aging 34, 1921.e9–1921.e15 (2013).

14. Holland D, Desikan RS, Dale AM, McEvoy LK, Alzheimer's Disease Neuroimaging Initiative, Rates of decline in Alzheimer disease decrease with age, PloS One 7, e42325 (2012). [PubMed: 22876315]

15. Wisse LEM, Das SR, Davatzikos C, Dickerson BC, Xie SX, Yushkevich PA, Wolk DA, Defining SNAP by cross-sectional and longitudinal definitions of neurodegeneration, NeuroImage Clin 18, 407–412 (2018). [PubMed: 29487798]

16. LaPoint MR, Chhatwal JP, Sepulcre J, Johnson KA, Sperling RA, Schultz AP, The association between tau PET and retrospective cortical thinning in clinically normal elderly, NeuroImage 157, 612–622 (2017). [PubMed: 28545932]

17. Das SR, Xie L, Wisse LEM, Ittyerah R, Tustison NJ, Dickerson BC, Yushkevich PA, Wolk DA, Alzheimer's Disease Neuroimaging Initiative, Longitudinal and cross-sectional structural magnetic resonance imaging correlates of AV-1451 uptake, Neurobiol. Aging 66, 49–58 (2018). [PubMed: 29518752]

18. Leung KK, Bartlett JW, Barnes J, Manning EN, Ourselin S, Fox NC, Cerebral atrophy in mild cognitive impairment and Alzheimer disease, Neurology 80, 648–654 (2013). [PubMed: 23303849]

19. Sabuncu MR, Desikan RS, Sepulcre J, Yeo BTT, Liu H, Schmansky NJ, Reuter M, Weiner MW, Buckner RL, Sperling RA, Fischl B, for the A. D. N. Initiative, The Dynamics of Cortical and Hippocampal Atrophy in Alzheimer Disease, Arch. Neurol 68, 1040–1048 (2011). [PubMed: 21825241]

20. Cedarbaum JM, Jaros M, Hernandez C, Coley N, Andrieu S, Grundman M, Vellas B, Alzheimer's Disease Neuroimaging Initiative, Rationale for use of the Clinical Dementia Rating Sum of Boxes as a primary outcome measure for Alzheimer's disease clinical trials, Alzheimers Dement. J. Alzheimers Assoc 9, S45–55 (2013).
21. Gorno-Tempini ML, Hillis AE, Weintraub S, Kertesz A, Mendez M, Cappa SF, Ogar JM, Rohrer JD, Black S, Boeve BF, Manes F, Dronkers NF, Vandenberghe R, Rascovsky K, Patterson K, Miller BL, Knopman DS, Hodges JR, Mesulam MM, Grossman M, Classification of primary progressive aphasia and its variants, Neurology 76, 1006–1014 (2011). [PubMed: 21325651]
22. Crutch SJ, Schott JM, Rabinovici GD, Murray M, Snowden JS, van der Flier WM, Dickerson BC, Vandenberghe R, Ahmed S, Bak TH, Boeve BF, Butler C, Cappa SF, Ceccaldi M, de Souza LC, Dubois B, Felician O, Galasko D, Graff-Radford J, Graff-Radford NR, Hof PR, Krolak-Salmon P, Lehmann M, Magnin E, Mendez MF, Nestor PJ, Onyike CU, Pelak VS, Pijnenburg Y, Primativo S, Rossor MN, Ryan NS, Scheltens P, Shakespeare TJ, Suárez González A, Tang-Wai DF, Yong KXX, Carrillo M, Fox NC, Alzheimer's Association ISTAART Atypical Alzheimer's Disease and Associated Syndromes Professional Interest Area, Consensus classification of posterior cortical atrophy, Alzheimers Dement. J. Alzheimers Assoc 13, 870–884 (2017).
23. La Joie R, Bejanin A, Fagan AM, Ayakta N, Baker SL, Bourakova V, Boxer AL, Cha J, Karydas A, Jerome G, Maass A, Mensing A, Miller ZA, O'Neil JP, Pham J, Rosen HJ, Tsai R, Visani AV, Miller BL, Jagust WJ, Rabinovici GD, Associations between [18F]AV1451 tau PET and CSF measures of tau pathology in a clinical sample, Neurology 90, e282–e290 (2018). [PubMed: 29282337]
24. Ashburner J, Ridgway GR, Symmetric Diffeomorphic Modeling of Longitudinal Structural MRI, Front. Neurosci 6 (2013), doi:10.3389/fnins.2012.00197.
25. Potvin O, Dieumegarde L, Duchesne S, Alzheimer's Disease Neuroimaging Initiative, Normative morphometric data for cerebral cortical areas over the lifetime of the adult human brain, NeuroImage 156, 315–339 (2017). [PubMed: 28512057]
26. Bejanin A, La Joie R, Landeau B, Belliard S, de La Sayette V, Eustache F, Desgranges B, Chételat G, Distinct Interplay Between Atrophy and Hypometabolism in Alzheimer's Versus Semantic Dementia, Cereb. Cortex N. Y. N 1991 (2018), doi:10.1093/cercor/bhy069.
27. Harrison TM, La Joie R, Maass A, Baker SL, Swinnerton K, Fenton L, Mellinger TJ, Edwards L, Pham J, Miller BL, Rabinovici GD, Jagust WJ, Longitudinal tau accumulation and atrophy in aging and alzheimer disease, Ann. Neurol 85, 229–240 (2019). [PubMed: 30597624]
28. Wahlund L-O, Blennow K, Cerebrospinal fluid biomarkers for disease stage and intensity in cognitively impaired patients, Neurosci. Lett 339, 99–102 (2003). [PubMed: 12614904]
29. Henneman WJP, Vrenken H, Barnes J, Sluimer IC, Verwey NA, Blankenstein MA, Klein M, Fox NC, Scheltens P, Barkhof F, van der Flier WM, Baseline CSF p-tau levels independently predict progression of hippocampal atrophy in Alzheimer disease, Neurology 73, 935–940 (2009). [PubMed: 19770469]
30. Tarawneh R, Head D, Allison S, Buckles V, Fagan AM, Ladenson JH, Morris JC, Holtzman DM, Cerebrospinal Fluid Markers of Neurodegeneration and Rates of Brain Atrophy in Early Alzheimer Disease, JAMA Neurol 72, 656–665 (2015). [PubMed: 25867677]
31. Fjell AM, Walhovd KB, Fennema-Notestine C, McEvoy LK, Hagler DJ, Holland D, Brewer JB, Dale AM, CSF Biomarkers in Prediction of Cerebral and Clinical Change in Mild Cognitive Impairment and Alzheimer's Disease, J. Neurosci 30, 2088–2101 (2010). [PubMed: 20147537]
32. Schuff N, Woerner N, Boreta L, Kornfield T, Shaw LM, Trojanowski JQ, Thompson PM, Jack CR, Weiner MW, Alzheimer's Disease Neuroimaging Initiative, MRI of hippocampal volume loss in early Alzheimer's disease in relation to ApoE genotype and biomarkers, Brain J. Neurol 132, 1067–1077 (2009).
33. Sluimer JD, Bouwman FH, Vrenken H, Blankenstein MA, Barkhof F, van der Flier WM, Scheltens P, Whole-brain atrophy rate and CSF biomarker levels in MCI and AD: a longitudinal study, Neurobiol. Aging 31, 758–764 (2010). [PubMed: 18692273]
34. Mattsson N, Schöll M, Strandberg O, Smith R, Palmqvist S, Insel PS, Hägerström D, Ohlsson T, Zetterberg H, Jögi J, Blennow K, Hansson O, 18F-AV-1451 and CSF T-tau and P-tau as biomarkers in Alzheimer's disease, EMBO Mol. Med 9, 1212–1223 (2017). [PubMed: 28743782]

35. Chhatwal JP, Schultz AP, Marshall GA, Boot B, Gomez-Isla T, Dumurgier J, LaPoint M, Scherzer C, Roe AD, Hyman BT, Sperling RA, Johnson KA, Temporal T807 binding correlates with CSF tau and phospho-tau in normal elderly, Neurology 87, 920–926 (2016). [PubMed: 27473132]
36. Schott JM, Bartlett JW, Barnes J, Leung KK, Ourselin S, Fox NC, Reduced sample sizes for atrophy outcomes in Alzheimer's disease trials: baseline adjustment, Neurobiol. Aging 31, 1452–1462.e2 (2010). [PubMed: 20620665]
37. Cash DM, Rohrer JD, Ryan NS, Ourselin S, Fox NC, Imaging endpoints for clinical trials in Alzheimer's disease, Alzheimers Res. Ther 6, 87 (2014). [PubMed: 25621018]
38. Whitwell JL, Dickson DW, Murray ME, Weigand SD, Tosakulwong N, Senjem ML, Knopman DS, Boeve BF, Parisi JE, Petersen RC, Jack CR, Josephs KA, Neuroimaging correlates of pathologically defined subtypes of Alzheimer's disease: a case-control study, Lancet Neurol 11, 868–877 (2012). [PubMed: 22951070]
39. Zhang X, Mormino EC, Sun N, Sperling RA, Sabuncu MR, Yeo BTT, Alzheimer's Disease Neuroimaging Initiative, Bayesian model reveals latent atrophy factors with dissociable cognitive trajectories in Alzheimer's disease, Proc. Natl. Acad. Sci. U. S. A 113, E6535–E6544 (2016). [PubMed: 27702899]
40. Murray ME, Graff-Radford NR, Ross OA, Petersen RC, Duara R, Dickson DW, Neuropathologically defined subtypes of Alzheimer's disease with distinct clinical characteristics: a retrospective study, Lancet Neurol 10, 785–796 (2011). [PubMed: 21802369]
41. Gutman BA, Wang Y, Yanovsky I, Hua X, Toga AW, Jack CR, Weiner MW, Thompson PM, Empowering Imaging Biomarkers of Alzheimer's Disease, Neurobiol. Aging 36 Suppl 1, S69–S80 (2015). [PubMed: 25260848]
42. Edland SD, Ard MC, Sridhar J, Cobia D, Martersteck A, Mesulam MM, Rogalski EJ, Proof of concept demonstration of optimal composite MRI endpoints for clinical trials, Alzheimers Dement. N. Y. N 2, 177–181 (2016).
43. La Joie R, Perrotin A, Barré L, Hommet C, Mézenge F, Ibazizene M, Camus V, Abbas A, Landeau B, Guilloteau D, de La Sayette V, Eustache F, Desgranges B, Chételat G, Region-specific hierarchy between atrophy, hypometabolism, and β-amyloid (Aβ) load in Alzheimer's disease dementia, J. Neurosci. Off. J. Soc. Neurosci 32, 16265–16273 (2012).
44. Chételat G, Villemagne VL, Bourgeat P, Pike KE, Jones G, Ames D, Ellis KA, Szoeke C, Martins RN, O'Keefe GJ, Salvado O, Masters CL, Rowe CC, Relationship between atrophy and beta-amyloid deposition in Alzheimer disease, Ann. Neurol 67, 317–324 (2010). [PubMed: 20373343]
45. Falke E, Nissanov J, Mitchell TW, Bennett DA, Trojanowski JQ, Arnold SE, Subicular dendritic arborization in Alzheimer's disease correlates with neurofibrillary tangle density, Am. J. Pathol 163, 1615–1621 (2003). [PubMed: 14507668]
46. Gómez-Isla T, Hollister R, West H, Mui S, Growdon JH, Petersen RC, Parisi JE, Hyman BT, Neuronal loss correlates with but exceeds neurofibrillary tangles in Alzheimer's disease, Ann. Neurol 41, 17–24 (1997). [PubMed: 9005861]
47. Dupont A-C, Largeau B, Santiago Ribeiro MJ, Guilloteau D, Tronel C, Arlicot N, Translocator Protein-18 kDa (TSPO) Positron Emission Tomography (PET) Imaging and Its Clinical Impact in Neurodegenerative Diseases, Int. J. Mol. Sci 18 (2017), doi:10.3390/ijms18040785.
48. Bourgeat P, Chételat G, Villemagne VL, Fripp J, Raniga P, Pike K, Acosta O, Szoeke C, Ourselin S, Ames D, Ellis KA, Martins RN, Masters CL, Rowe CC, Salvado O, Beta-amyloid burden in the temporal neocortex is related to hippocampal atrophy in elderly subjects without dementia, Neurology 74, 121–127 (2010). [PubMed: 20065247]
49. Klupp E, Grimmer T, Tahmasian M, Sorg C, Yakushev I, Yousefi BH, Drzezga A, Förster S, Prefrontal hypometabolism in Alzheimer disease is related to longitudinal amyloid accumulation in remote brain regions, J. Nucl. Med. Off. Publ. Soc. Nucl. Med 56, 399–404 (2015).
50. Josephs KA, Dickson DW, Tosakulwong N, Weigand SD, Murray ME, Petrucelli L, Liesinger AM, Senjem ML, Spychalla AJ, Knopman DS, Parisi JE, Petersen RC, Jack CR, Whitwell JL, Rates of hippocampal atrophy and presence of post-mortem TDP-43 in patients with Alzheimer's disease: a longitudinal retrospective study, Lancet Neurol 16, 917–924 (2017). [PubMed: 28919059]
51. Whitwell JL, Graff-Radford J, Tosakulwong N, Weigand SD, Machulda MM, Senjem ML, Spychalla AJ, Vemuri P, Jones DT, Drubach DA, Knopman DS, Boeve BF, Ertekin-Taner N,

Petersen RC, Lowe VJ, Jack CR, Josephs KA, Imaging correlations of tau, amyloid, metabolism, and atrophy in typical and atypical Alzheimer's disease, Alzheimers Dement. J. Alzheimers Assoc 14, 1005–1014 (2018).

52. Gerritsen AAJ, Bakker C, Verhey FRJ, de Vugt ME, Melis RJF, Koopmans RTCM, 4C study team, Prevalence of Comorbidity in Patients With Young-Onset Alzheimer Disease Compared With Late-Onset: A Comparative Cohort Study, J. Am. Med. Dir. Assoc 17, 318–323 (2016). [PubMed: 26778489]
53. Rabinovici GD, Carrillo MC, Forman M, DeSanti S, Miller DS, Kozauer N, Petersen RC, Randolph C, Knopman DS, Smith EE, Isaac M, Mattsson N, Bain LJ, Hendrix JA, Sims JR, Multiple comorbid neuropathologies in the setting of Alzheimer's disease neuropathology and implications for drug development, Alzheimers Dement. Transl. Res. Clin. Interv 3, 83–91 (2017).
54. James BD, Bennett DA, Boyle PA, Leurgans S, Schneider JA, Dementia from Alzheimer disease and mixed pathologies in the oldest old, JAMA 307, 1798–1800 (2012). [PubMed: 22550192]
55. Marquié M, Verwer EE, Meltzer AC, Kim SJW, Agüero C, Gonzalez J, Makaretz SJ, Siao Tick Chong M, Ramanan P, Amaral AC, Normandin MD, Vanderburg CR, Gomperts SN, Johnson KA, Frosch MP, Gómez-Isla T, Lessons learned about [F-18]-AV-1451 off-target binding from an autopsy-confirmed Parkinson's case, Acta Neuropathol. Commun 5, 75 (2017). [PubMed: 29047416]
56. Sander K, Lashley T, Gami P, Gendron T, Lythgoe MF, Rohrer JD, Schott JM, Revesz T, Fox NC, Årstad E, Characterization of tau positron emission tomography tracer [18F]AV-1451 binding to postmortem tissue in Alzheimer's disease, primary tauopathies, and other dementias, Alzheimers Dement. J. Alzheimers Assoc 12, 1116–1124 (2016).
57. Choi JY, Cho H, Ahn SJ, Lee JH, Ryu YH, Lee MS, Lyoo CH, Off-Target 18F-AV-1451 Binding in the Basal Ganglia Correlates with Age-Related Iron Accumulation, J. Nucl. Med. Off. Publ. Soc. Nucl. Med 59, 117–120 (2018).
58. Baker SL, Maass A, Jagust WJ, Considerations and code for partial volume correcting [18F]-AV-1451 tau PET data, Data Brief 15, 648–657 (2017). [PubMed: 29124088]
59. Lockhart SN, Ayakta N, Winer JR, La Joie R, Rabinovici GD, Jagust WJ, Elevated (18)F-AV-1451 PET tracer uptake detected in incidental imaging findings, Neurology 88, 1095–1097 (2017). [PubMed: 28188303]
60. Tsai RM, Bejanin A, Lesman-Segev O, LaJoie R, Visani A, Bourakova V, O'Neil JP, Janabi M, Baker S, Lee SE, Perry DC, Bajorek L, Karydas A, Spina S, Grinberg LT, Seeley WW, Ramos EM, Coppola G, Gorno-Tempini ML, Miller BL, Rosen HJ, Jagust W, Boxer AL, Rabinovici GD, 18F-flortaucipir (AV-1451) tau PET in frontotemporal dementia syndromes, Alzheimers Res. Ther 11, 13 (2019). [PubMed: 30704514]
61. Bakota L, Brandt R, Tau Biology and Tau-Directed Therapies for Alzheimer's Disease, Drugs 76, 301–313 (2016). [PubMed: 26729186]
62. McKhann GM, Knopman DS, Chertkow H, Hyman BT, Jack CR Jr, Kawas CH, Klunk WE, Koroshetz WJ, Manly JJ, Mayeux R, Mohs RC, Morris JC, Rossor MN, Scheltens P, Carrillo MC, Thies B, Weintraub S, Phelps CH, The diagnosis of dementia due to Alzheimer's disease: recommendations from the National Institute on Aging-Alzheimer's Association workgroups on diagnostic guidelines for Alzheimer's disease, Alzheimers Dement. J. Alzheimers Assoc 7, 263–269 (2011).
63. Albert MS, DeKosky ST, Dickson D, Dubois B, Feldman HH, Fox NC, Gamst A, Holtzman DM, Jagust WJ, Petersen RC, Snyder PJ, Carrillo MC, Thies B, Phelps CH, The diagnosis of mild cognitive impairment due to Alzheimer's disease: recommendations from the National Institute on Aging-Alzheimer's Association workgroups on diagnostic guidelines for Alzheimer's disease, Alzheimers Dement. J. Alzheimers Assoc 7, 270–279 (2011).
64. Rabinovici GD, Rosen HJ, Alkalay A, Kornak J, Furst AJ, Agarwal N, Mormino EC, O'Neil JP, Janabi M, Karydas A, Growdon ME, Jang JY, Huang EJ, Dearmond SJ, Trojanowski JQ, Grinberg LT, Gorno-Tempini ML, Seeley WW, Miller BL, Jagust WJ, Amyloid vs FDG-PET in the differential diagnosis of AD and FTLD, Neurology 77, 2034–2042 (2011). [PubMed: 22131541]
65. Diedrichsen J, Balsters JH, Flavell J, Cussans E, Ramnani N, A probabilistic MR atlas of the human cerebellum, NeuroImage 46, 39–46 (2009). [PubMed: 19457380]

66. Maass A, Landau S, Baker SL, Horng A, Lockhart SN, La Joie R, Rabinovici GD, Jagust WJ, Alzheimer's Disease Neuroimaging Initiative, Comparison of multiple tau-PET measures as biomarkers in aging and Alzheimer's disease, NeuroImage 157, 448–463 (2017). [PubMed: 28587897]

67. Hammers A, Allom R, Koepp MJ, Free SL, Myers R, Lemieux L, Mitchell TN, Brooks DJ, Duncan JS, Three-dimensional maximum probability atlas of the human brain, with particular reference to the temporal lobe, Hum. Brain Mapp 19, 224–247 (2003). [PubMed: 12874777]

68. Girard H, Potvin O, Nugent S, Dallaire-Théroux C, Cunnane S, Duchesne S, Alzheimer's Disease Neuroimaging Initiative, Faster progression from MCI to probable AD for carriers of a single-nucleotide polymorphism associated with type 2 diabetes, Neurobiol. Aging 64, 157.e11–157.e17 (2018).

69. Pernet CR, Wilcox R, Rousselet GA, Robust correlation analyses: false positive and power validation using a new open source matlab toolbox, Front. Psychol 3, 606 (2012). [PubMed: 23335907]

70. Xia M, Wang J, He Y, BrainNet Viewer: A Network Visualization Tool for Human Brain Connectomics, PLOS ONE 8, e68910 (2013). [PubMed: 23861951]

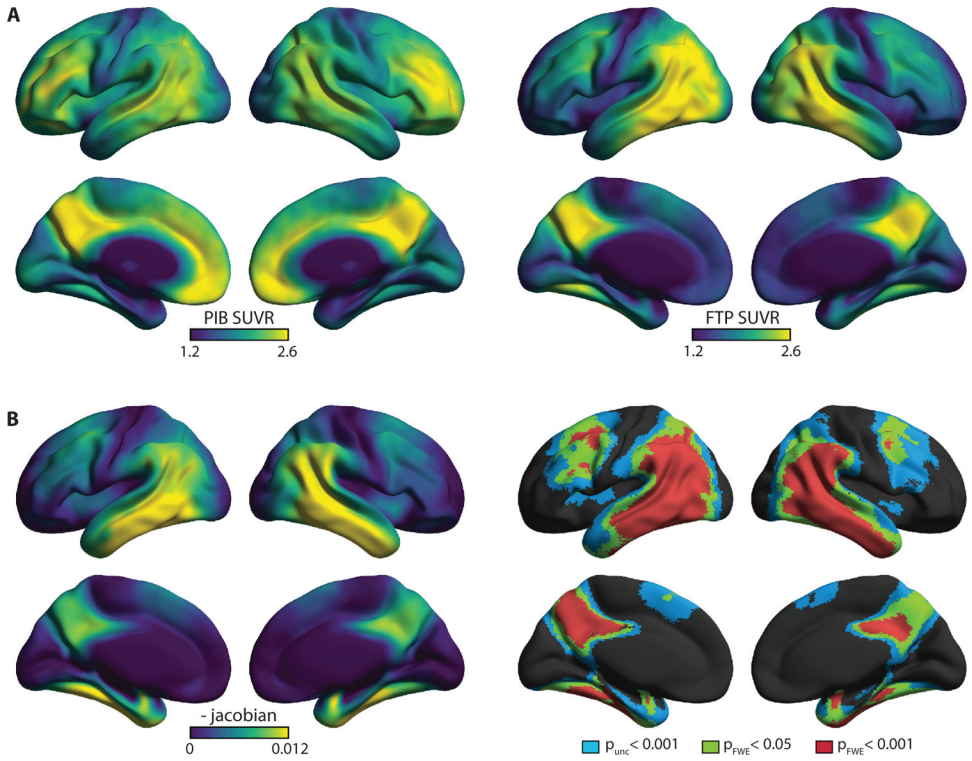


**Figure 1. Voxelwise patterns at the group level.**

A. Group-average PET SUVR maps at baseline.

B. Voxelwise pattern of longitudinal cortical atrophy. Left: average of 32 reversed GM-masked and smoothed reversed jacobian maps (higher value means higher rate of atrophy). Right: statistical map corresponding to a voxelwise one-sample t-test including the 32 individual maps, showing areas of significant atrophy (reversed jacobians > 0) based on three increasingly conservative thresholds ($p_{uncorrected} < 0.001$, Family-wise error (FWE) corrected $p_{FWE} < 0.05$ and $p_{FWE} < 0.001$ at the voxel level; all three with a $p_{FWE} < 0.05$ at the cluster level).

All maps are available for visualization at https://neurovault.org/collections/WLDODMCY/

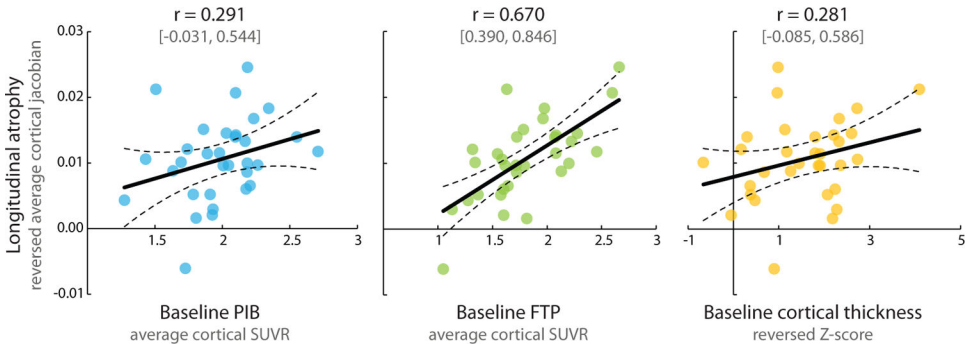


**Figure 2. Bivariate associations between baseline measures and subsequent atrophy across the 32 patients.**

95% Confidence Intervals (95%CI) were computed using bootstrapping with 5,000 permutations. Details about the statistical analyses, including a multiple regression with all three baseline predictors are available in the result section and Table S1.

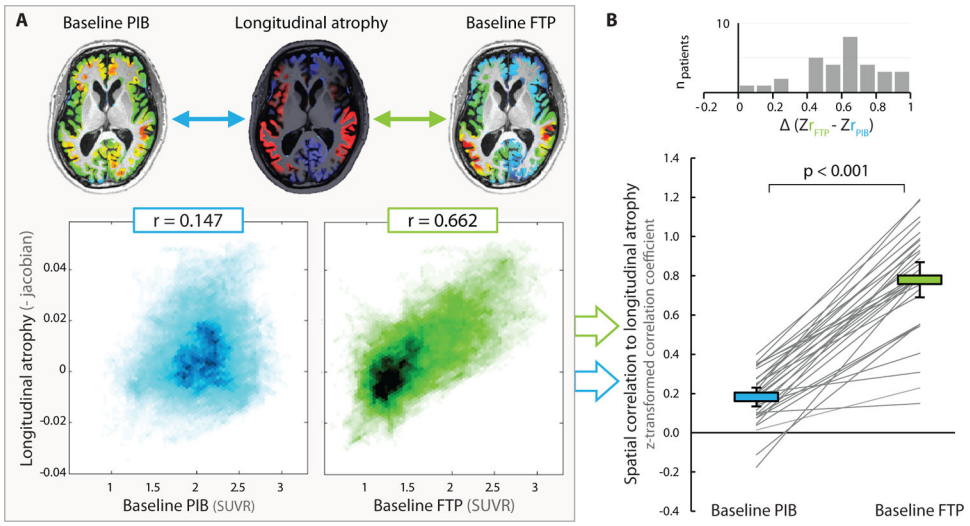


**Figure 3. Voxelwise spatial correlations between baseline PET patterns and the topography of subsequent atrophy.**

A. Analyses conducted at the individual patient level to quantify the similarity between patterns of PET SUVR at baseline and maps of longitudinal atrophy (reversed jacobians). The images used for illustration correspond to a patient with close-to-average values. For each patient, correlations were assessed on all voxels of the cortex (see Figure S1 for details about specific image preprocessing steps).

B. Group level analyses. Resulting correlation coefficients were z-transformed to be analyzed at the group level. Gray lines show individual patients while colored bars indicate average z-transformed coefficients (with 95% confidence intervals). P value corresponds to two-tailed paired t-test. The top panel shows the histogram of the difference between z-transformed spatial correlation coefficients between PIB and atrophy and FTP and atrophy across all 32 patients, highlighting that the latter was higher than the former in all 32 cases.

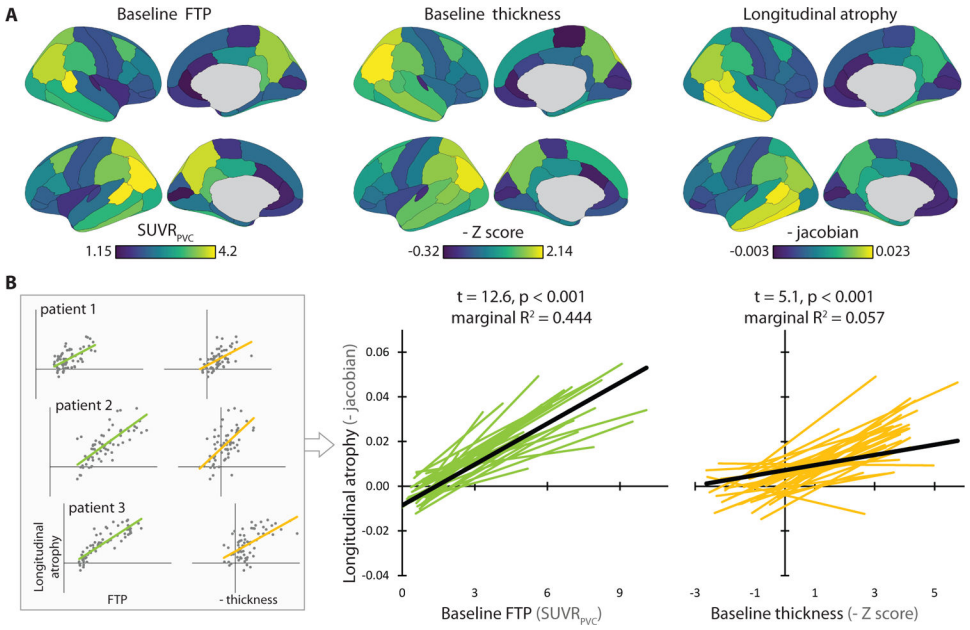


**Figure 4. Relative contribution of baseline partial volume corrected FTP-PET and baseline thickness patterns to predict the topography of subsequent atrophy using FreeSurfer-defined cortical regions of interest.**

A. Group average values in the 68 FreeSurfer cortical regions of interest (ROI). . The colorscale was adapted to the range of values of each modality to best illustrate regional variations. $SUVR_{PVC}$: Partial Volume-Corrected Standardized Uptake Value Ratio.

B. Spatial associations between patterns of baseline FTP-$SUVR_{PVC}$, thickness, and longitudinal atrophy were conducted for each patient based on the 68 ROI, as illustrated in the left panel. The spaghetti plots on the right illustrate the 32 regression lines obtained at the patient level for each pair of variables. The statistical indices on top of each spaghetti plot are related indicate the results of linear mixed effect models (LMEMs) to predict reverse jacobians; separate models were run with each of the two baseline variables as a predictor. A full model included both predictors together are described in the result section and in Table S2.

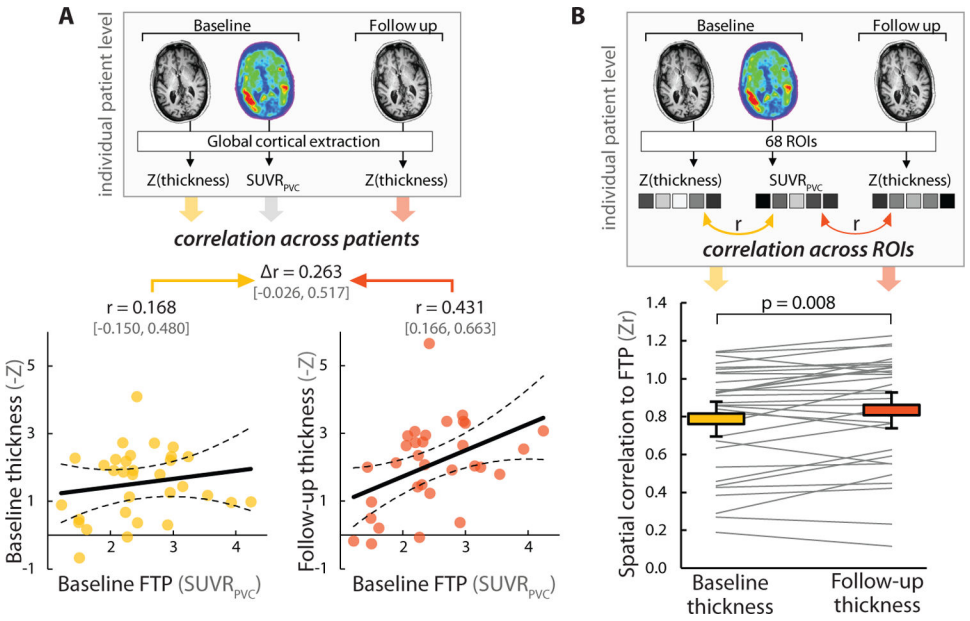


**Figure 5. Association between baseline FTP-PET and cortical thickness at baseline and follow-up**

A. Association between baseline global cortical partial volume-corrected (PVC) FTP-SUVR values and cortical thickness at baseline (yellow) and follow-up (orange) across patients. Cortical thickness measures were Z-scored based on normative data and reversed so higher values indicate more neurodegeneration. 95% confidence intervals are based on bootstrap with 5,000 permutations.

B. Spatial similarity between FTP-$SUVR_{PVC}$ and low cortical thickness at each time point was assessed at the single patient level using a correlation approach based on Freesurfer regions of interest (top panel). Cortical thickness was extracted from 68 FreeSurfer cortical ROIs, transformed into a Z-score using normative data, and reversed to higher values indicate more neurodegeneration; FTP-$SUVR_{PVC}$ values were extracted from each ROIs. Correlations were Fisher z-transformed to be analyzed at the group level (bottom panel). Each gray line represents a single patient and color bars illustrate group averages with bootstrap 95% confidence intervals. P value corresponds to a paired t-test, showing that patterns of baseline FTP binding are more similar to patterns of low cortical thickness at follow up than baseline.

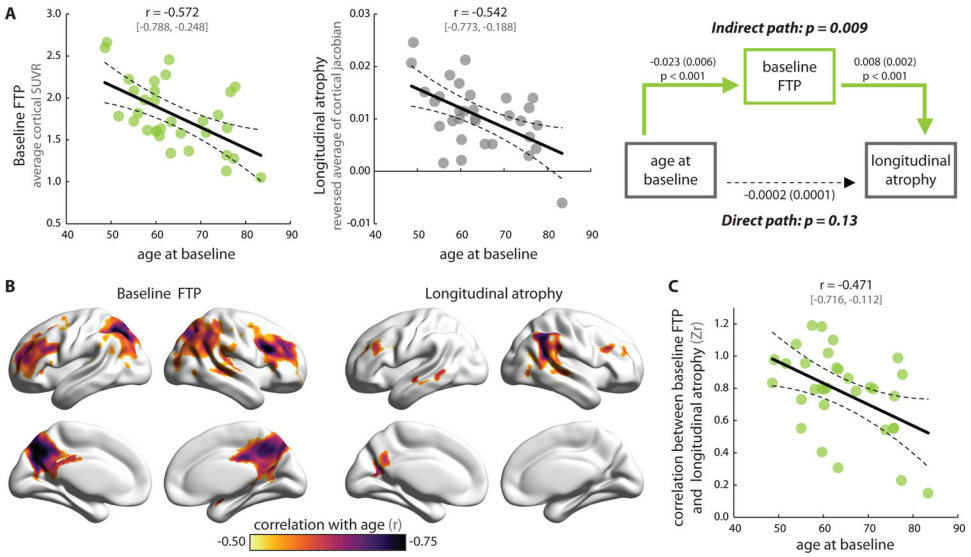


**Figure 6. Effect of patient age on baseline tau pathology and subsequent atrophy.**

A. Association between patient age and global cortical FTP-SUVR at baseline and longitudinal atrophy; see Figure S5 for associations between age and other variables. Mediation analysis showed that baseline cortical FTP-SUVR mediated the effect of age on longitudinal atrophy; see Figure S6 for the (non-significant) mediation models conducted with baseline PIB and baseline thickness instead of baseline FTP.

B. Voxelwise analyses showing the regional associations between increasing patient's age and lower FTP-SUVr or atrophy rates (see Figure S7 for unthresholded maps and https://neurovault.org/collections/WLDODMCY/ to access the 3D maps)

C. Association between patient's age and the topographical similarity between patterns of baseline FTP-SUVR and subsequent atrophy measured using voxelwise spatial correlation (as described in Figure 3); see Figure S5 for similar plot with PIB.

**Table 1.**

Patients included in the analyses.

| | |
|---|---|
| Sex: $n_{female}$ / $n_{male}$ | 21 / 11 |
| Age at baseline | 64 ± 9 [49, 83] |
| Education | 17 ± 3 [12, 24] |
| APOE4 alleles: $n_0$ / $n_1$ / $n_2$ ($n_{missing}$) | 14 / 13 / 3 (2) |
| MMSE at baseline | 24 ± 4 [14, 30] |
| CDR-SB at baseline | 3.8 ± 2 [0, 8] |
| Baseline to follow-up MRI (months) | 15 ± 3 [10, 24] |
| Baseline MRI to FTP-PET (months) | 1.8 ± 2.2 [0, 7.7] |
| Baseline MRI to PIB-PET (months) | 1.6 ± 2.3 [0, 7.7] |

For continuous variables, mean ± SD [min-max] is indicated. MMSE: Mini Mental State Examination; CDR-SB: Clinical Dementia Rating scale – Sum of Boxes.